NASA/TM–2012-208641 / Vol 9

ICESat (GLAS) Science Processing Software Document Series

The Algorithm Theoretical Basis Document for Tidal Corrections

Helen A. Fricker, Jeff R. Ridgway, Jean-Bernard Minster, Donghi Yi, Charles R. Bentley

National Aeronautics and
Space Administration

Goddard Space Flight Center
Greenbelt, Maryland 20771

November 2012

NASA STI Program ... in Profile

Since its founding, NASA has been dedicated to the advancement of aeronautics and space science. The NASA scientific and technical information (STI) program plays a key part in helping NASA maintain this important role.

The NASA STI program operates under the auspices of the Agency Chief Information Officer. It collects, organizes, provides for archiving, and disseminates NASA's STI. The NASA STI program provides access to the NASA Aeronautics and Space Database and its public interface, the NASA Technical Report Server, thus providing one of the largest collections of aeronautical and space science STI in the world. Results are published in both non-NASA channels and by NASA in the NASA STI Report Series, which includes the following report types:

- TECHNICAL PUBLICATION. Reports of completed research or a major significant phase of research that present the results of NASA Programs and include extensive data or theoretical analysis. Includes compilations of significant scientific and technical data and information deemed to be of continuing reference value. NASA counterpart of peer-reviewed formal professional papers but has less stringent limitations on manuscript length and extent of graphic presentations.
- TECHNICAL MEMORANDUM. Scientific and technical findings that are preliminary or of specialized interest, e.g., quick release reports, working papers, and bibliographies that contain minimal annotation. Does not contain extensive analysis.
- CONTRACTOR REPORT. Scientific and technical findings by NASA-sponsored contractors and grantees.
- CONFERENCE PUBLICATION. Collected papers from scientific and technical conferences, symposia, seminars, or other meetings sponsored or co-sponsored by NASA.
- SPECIAL PUBLICATION. Scientific, technical, or historical information from NASA programs, projects, and missions, often concerned with subjects having substantial public interest.
- TECHNICAL TRANSLATION. English-language translations of foreign scientific and technical material pertinent to NASA's mission.

Specialized services also include organizing and publishing research results, distributing specialized research announcements and feeds, providing help desk and personal search support, and enabling data exchange services. For more information about the NASA STI program, see the following:

- Access the NASA STI program home page at http://www.sti.nasa.gov
- E-mail your question via the Internet to help@sti.nasa.gov
- Fax your question to the NASA STI Help Desk at 443-757-5803
- Phone the NASA STI Help Desk at 443-757-5802
- Write to:

  NASA STI Help Desk
  NASA Center for AeroSpace Information
  7115 Standard Drive
  Hanover, MD 21076-1320

NASA/TM–2012-208641 / Vol 9

ICESat (GLAS) Science Processing Software Document Series

The Algorithm Theoretical Basis Document for Tidal Corrections

Helen A. Fricker, Jeff R. Ridgway, Jean-Bernard Minster
Scripps Institution of Oceanography, La Jolla, CA

Donghui Yi, SGT, Inc., Greenbelt, MD

Charles R. Bentley, University of Wisconsin, Madison, WI

National Aeronautics and
Space Administration

Goddard Space Flight Center
Greenbelt, Maryland 20771

November 2012

Level of Review: This material has been technically reviewed by technical management

Available from:
NASA Center for AeroSpace Information
7115 Standard Drive
Hanover, MD 21076-1320

National Technical Information Service
5285 Port Royal Road
Springfield, VA 22161 Price Code: A17

Table of Contents

List of Figures

List of Tables

1. Introduction

This Algorithm Theoretical Basis Document deals with the tidal corrections that need to be applied to range measurements made by the Geoscience Laser Altimeter System (GLAS). These corrections result from the action of ocean tides and Earth tides which lead to deviations from an equilibrium surface. Since the effect of tides is dependent of the time of measurement, it is necessary to remove the instantaneous tide components when processing altimeter data, so that all measurements are made to the equilibrium surface.

The three main tide components to consider are the ocean tide, the solid-earth tide and the ocean loading tide. There are also long period ocean tides and the pole tide. The approximate magnitudes of these components are illustrated in Table 1, together with estimates of their uncertainties (i.e. the residual error after correction). All of these components are important for GLAS measurements over the ice sheets since centimeter-level accuracy for surface elevation change detection is required. The effect of each tidal component is to be removed by approximating their magnitude using tidal prediction models. Conversely, assimilation of GLAS measurements into tidal models will help to improve them, especially at high latitudes.

2. Background

The Antarctic and Greenland ice sheets contain enough water to produce a 72-m rise in sea-level if they were to melt (*Oerlemans*, 1993). For this reason alone, we need to understand how Antarctica and Greenland will respond to climate change. During the present century, sea-level has risen at an average rate of 1.0-2.0 mm yr^{-1} (*Warrick*, 1993). Part of the sea level rise can be explained by ocean thermal expansion and the melting of glaciers and small ice caps and, perhaps, net mass loss to the Greenland ice sheet. The amount of snow that falls each year on the grounded Antarctic ice is equivalent to about 5 mm yr^{-1} of global sea level change (*Jacobs*, 1992), so annual variation of snow accumulation on the Antarctic ice sheet can have a measurable effect on sea level. Without independent knowledge of the contribution of the Antarctic ice sheet, there remains a major uncertainty in understanding sea level change (*Warrick and Oerlemans*, 1990). To fix ideas, assuming that half of the sea-level rise, i.e. 0.5-1.0 mm yr^{-1}, comes from a mass loss to the Antarctic ice sheet, then the mean elevation of Antarctica would need to drop at a rate of about 15-30 mm yr^{-1}. This estimate ignores the potential contributions of other phenomena, such as post-glacial rebound.

Satellite altimeters can be used to monitor the volume of the polar ice sheets. Substantial progress in studying polar mass balance has been sustained by the use of satellite radar altimeters (*Brenner et al*, 1983, *Zwally et al,* 1989, *Zwally*, 1989, *Partington et al,* 1991, *Bentley and Sheehan*, 1992, *Lingle et al*, 1994, *Yi et al,* 1997). However the precision of the satellite radar altimeters is limited by surface slope because of the large radar footprint (*Brenner et al,* 1983), imperfect understanding of the microwave penetration to the subsnow surface (*Ridley and Partington,* 1988, *Yi and Bentley,* 1997), and inadequate accuracy of satellite orbits (*Haines et al,* 1994). The Geoscience Laser Altimeter System (GLAS) (*Schutz*, 1995), designed primarily for measuring the surface elevation of the polar ice sheets, has a much smaller footprint of about 70 m which will reduce the surface slope effect and benefits from an on-board GPS which will give an orbit accuracy of ±50 mm.

Ocean tides and solid earth tides have been taken into account in processing the satellite

radar altimetry data (e.g. *Zwally et al,* 1990). However, the smaller vertical displacement caused by the ocean tidal loading has not previously been given much attention. This is because the precision of satellite radar altimeters over land is of the order of several tens of centimeters while the vertical displacement load tide is only of the order of several tens of millimeters even along the coast. Ocean loading effects only become important when the surface elevation measurements require centimeter-level precision. To determine surface elevation accurately and to detect surface elevation change, it is important to estimate the ocean tidal loading effects and apply an ocean tidal loading correction to the surface elevation measurement.

3. 'Standard' Tide Corrections

Several of the tide corrections listed in Table 1 will be removed from GLAS range measurements by applying 'standard' models that have been successfully used for previous satellite altimeter missions such as ERS-1, ERS-2 and TOPEX/Poseidon. These corrections are the solid earth tide, long-period tides and pole tide.

- **Solid Earth Tide** The solid earth tide is the periodic movement of the Earth's crust caused by gravitational interactions between the Sun, Moon and Earth. The magnitude of this tide is $\pm$30cm, and its effect should be removed for GLAS through modeling, in the same way as it was for TOPEX/Poseidon. This was done using TOPEX/Poseidon document "g1062" (with the tested algorithm 'TIDPOT.FOR')

- **Long-period Tides** Equilibrium long period tides are removed by models which are based on the Cartwright-Taylor-Edden tide potential. Any reliable code (such as subroutine 'lpeqmt', written by *Cartwright* (1990)) that is used for TOPEX/Poseidon should be used for its calculation for the GLAS records, independently of the diurnal/semidiurnal ocean tide model used. The non-equilibrium long-period tide should probably be ignored, as it is small and no model for it has yet been finalized.

- **Pole Tide** This tide results from polar motion has component periods mainly of 12 months and 14 months. It should be calculated for GLAS after TOPEX/Poseidon algorithm document g1063.

4. Ocean Tide Correction

4.1 Ocean Regions

Tides over the open ocean will be removed from GLAS range measurements by applying a ocean tide model. This tide model should ideally be global, include predictions for the Arctic and the Antarctic, and be familiar to the TOPEX/Poseidon software team. Two suitable models are CSR3.0 (*Eanes,* 1994; used for TOPEX/Poseidon) and FES95.2 (*Le Provost et al.,* 1998), and these two models compare fairly well in the open ocean *(Shum et al.,* 1997*)*. Although CSR3.0 was used for TOPEX/Poseidon, it is not reliable below 78°S. We therefore recommend that the FES95.2 model is adopted as the primary global model for GLAS ocean tide corrections. This is an improvement of the FES94.1 model as it assimilates into the hydrodynamic model the earlier empirical TOPEX/Poseidon CSR2.0 tidal solution using the representer methods developed by

Egbert et al. (1994). The CSR2.0 solutions were derived in 1994 at the University of Texas, from a two year time series of TOPEX/Poseidon data. The standard release of the FES95.2 solutions is 0.5° x 0.5° for ocean depths greater than 1000 m. The tidal correction at a specific location and time will be interpolated based on their location within this grid.

We also recommend that a second model be considered for application around Antarctica. This is the Circum-Antarctic Tidal Simulation model (CATS99.2), developed at the Earth and Space Science Center, Seattle, Washington by Laurence Padman (*Rignot et al.* 1999). The CATS99.2 model covers the entire globe south of 50°S, at a resolution of 0.25° in latitude (approximately 10 km around the Antarctic coast) and has been validated in the Weddell Sea region (*Robertson et al.* 1998) and at the front of the Filchner Ice Shelf (*Rignot et al.* 1999). The model comprises eight tidal constituents, five semidiurnal (M_2, S_2, K_2, N_2, and $2N_2$) and three diurnal (O_1, K_1, and Q_1). Incorporation of this model has the advantage that it is continuous at the boundary with the FES95.2 and would simply require a latitude switch so that this model is utilized below 50°S. However, it is noted that the process of 'matching' models at 50°S should be the object of careful analysis.

4.2 Ice Shelves and Glacier Tongues

The floating parts of the ice sheets (ice shelves and floating glacier tongues) are displaced vertically in response to ocean tides. To assess elevation change in these regions, the instantaneous tide component must be removed from the elevation measurement, such that all ice shelf elevations are referred to an equilibrium surface. Modeling the tidal displacement of the floating ice shelves in response to ocean tides is not straightforward. There is currently no one model that accurately described the complex response of the floating parts of the Antarctic ice sheet to ocean tides. The CATS99.2 model has been shown to perform well at the ice front of the Filchner Ice Shelf (*Rignot et al.* 1999), but still requires work in other areas. This model will be improved as more observations from ice shelf tides (e.g. from *in situ* GPS, GLAS) and information on sub-ice-shelf water column thickness become available *(Laurence Padman, personal communication, July 1999)*.

The vertical displacement of the ice shelves can be measured using kinematic GPS (e.g. *Vaughan 1994, 1995*) and static GPS (e.g. *Phillips et al. 1998*). For the Amery Ice Shelf, *Phillips et al* (*1998*) showed that the amplitude of the vertical tidal displacement at six sites on the central part of the ice shelf is the same as that predicted by a tide model for nearby Beaver Lake, provided by the National Tidal Facility, The Flinders University of South Australia. Static GPS observations collected on the Amery Ice Shelf during 1998-1999 have been processed in 1-hour segments within the GAMIT software *(Richard Coleman, personal communication, 1999)*. The results indicate that there is a phase lag between the Beaver Lake Tide Model and the tidal response of the Amery Ice Shelf, with the Amery Ice Shelf ahead by around 65 minutes at the northernmost site (near the ice front) and 45 minutes at the southernmost site (near the grounding zone). The distance between these sites is approximately 400 km. A three-years series of field campaigns is planned for 1999-2000, 2000-1 and 2001-2. It is intended to use GLAS data acquired during the 90-day verification and validation phase of ICESat to generate new models (or improve existing models) for the major floating ice shelves, and these results will be validated using *in situ* observations from the Amery Ice Shelf. In addition to the data collected on the Amery Ice Shelf, we also recommend that long time series of static GPS data are collected on other ice shelves (e.g. Ross Ice Shelf, Ronne Ice Shelf, Filchner Ice Shelf) for further validation of ice shelf tide models.

When available, these 'local' models can potentially be added into higher level GLAS data products by specifying a mask for each region. This remains a research issue.

4.3 Land/Ocean Mask

The resolution requirement for the Land/Ocean mask is higher for GLAS than it was for TOPEX/Poseidon. Application of a tidal model for GLAS requires a Land/Ocean mask that has a horizontal resolution of about 1 km. We recommend that:

1) the worldwide Generic Mapping Tool (GMT) database of *Wessel and Smith* (1996) be adopted. The implementation of Agnew (1996; see Section 4), has a resolution of 1/64 degree (1.7 km), saves disk space and is compatible with his load-tide software and is also recommended.

2) the Land/Ocean mask not be hard-coded but be stored as a readable file, which will be updated with more accurate values as they become available (e.g. for the floating ice extent of the Antarctic ice shelves). Sufficient flexibility should be programmed into the code such that higher-resolution versions of the land/ocean mask can be used as they are developed. Another consideration is the 'transition zone' of the Antarctic ice shelves. This is the region between the 'limit of flexure' i.e. the boundary between fully grounded and freely floating ice and the hydrostatic grounding line (the 'hinge line') which can extend for several kilometers *(Vaughan 1994)*. In this region, the ice does not respond freely to the ocean tides. Vaughan *(1995)* successfully modeled this as elastic plate flexure with an elastic modulus of about 0.88 GPa. However, we do not think that this should be calculated for incorporation into the GLAS records. This is a future topic of research and will be much improved with additional static GPS observations, information from Interferometric Synthetic Aperture Radar (InSAR) (e.g. *Rignot* 1998) and when GLAS data start becoming available.

5. Ocean-loading Tide

The mass of water concentrated by the ocean tidal bulge is sufficient to compress the Earth's lithosphere. As this mass is redistributed, elastic rebound of the lithosphere changes, and this is the ocean-loading tide. The vertical displacement caused by ocean-loading is of the order of several tens of millimeters in polar regions (Table 1), although it is primarily restricted to the vicinity of the coastline. Application of the ocean tidal loading correction will improve the accuracy of satellite laser altimeter measured surface elevation over the ice sheets, especially in the coastal areas.

5.1 Computation of Ocean Tidal Loading

Various methods have been used to compute tidal loading. *Baker* (1985) lists five of them: (1) the spherical harmonic expansion method; (2) the polygon method; (3) the template method; (4) the spherical disc method; and (5) the Green's function method. In this ATBD, the tidal loading is computed by the Green's function method (*Farrell*, 1972). *Agnew* (1996) produced a software package which makes it is easy to calculate tidal loading at a given point by using the Green's function and an ocean tide model. In Agnew's package, the ocean load tide L is given by

$$L(\theta', \lambda') = \int_0^{2\pi} \left(\int_0^{\pi} \rho H(\theta, \lambda) G_L(\Delta) S_L(\alpha) a^2 \sin(\theta) d\theta \right) d\lambda \qquad (1)$$

where Δ is the distance, α is the azimuth of the point with geographical coordinates (θ, λ) relative to the place of observation, which is at (θ', λ'); H is the tidal height at (θ, λ), ρ is ocean water density, and a is the radius of the earth. G_L is the mass loading Green's function and S_L is the combination of trigonometric functions needed to compute a vector or tensor load. The Green functions used are obtained from *Farrell* (1972). As stated in Section 3.1, the global tide model we propose to use for the open ocean is the FES95.2 model (*Le Provost et al* 1998), and we would like to leave scope to include the CATS99.2 model below 50°S. Both of these models are compatible with Agnew's (1996) code (Duncan Agnew, personal communication, July 1999). In fact, local high accuracy models for specific locations, such as shallow seas (e.g. North Sea, English Channel, etc), or areas such as the Amery ice shelf, can be accommodated as well.

5. 2 Algorithm Description

The displacement component at a location at a time *t* is given by (*McCarthy*, 1992)

$$\Delta c = \sum_j f_j A_j \cos(\omega_j t + \chi_j + \mu_j - \Phi_j) \qquad (2)$$

where f_j and μ_j depend on the longitude of the lunar node, A_j and Φ_j are the amplitude and phase for each displacement component, ω_j is the frequency of tide *j* and χ_j is the astronomical argument at t = 0. The three components of displacement (vertical, east-west, north-south) can be calculated by the above equation, but here we are only interested in the vertical displacement. χ_j is calculated using the program ARG described by *McCarthy* (1992). f_j and μ_j are calculated by the following relations for the eight largest constituents, which together account for over 90% of the tidal signal (*Doodson*, 1928):

$f_{m2} = 1.000 - 0.037 \cos(N)$

$f_{s2} = 1.0$

$f_{n2} = 1.000 - 0.037 \cos(N)$

$f_{k2} = 1.024 + 0.286 \cos(N) + 0.008 \cos(2N)$

$f_{k1} = 1.006 + 0.115 \cos(N) - 0.009 \cos(2N)$

$f_{o1} = 1.009 + 0.187 \cos(N) - 0.015 \cos(2N)$

$f_{p1} = 1.0$

$f_{q1} = 1.009 + 0.187 \cos(N) - 0.015 \cos(2N)$

$\mu_{m2} = -2.1° \sin(N)$

$\mu_{s2} = 0.0°$

$\mu_{n2} = -2.1° \sin(N)$

$\mu_{k2} = -17.7° \sin(N) + 0.7° \sin(2N)$

$\mu_{k1} = -8.9° \sin(N) + 0.7° \sin(2N)$

$$\mu_{o1} = 10.8° \sin(N) - 1.3° \sin(2N) + 0.2° \sin(3N)$$

$$\mu_{p1} = 0.0°$$

$$\mu_{q1} = 10.8° \sin(N) - 1.3° \sin(2N) + 0.2° \sin(3N)$$

$$N = (259.16° - 19.3282° (year-1900) - 0.0530° (day + leapyear))$$

Since the calculation of the amplitude and phase of a tidal constituent is relatively time consuming, an interpolation method on a gridded set of pre-calculated results is used instead.The load tide varies smoothly, so it can be interpolated in space and time with negligible error. We calculate the tidal loading at a point (x, y) by first determining its value at the four nearest neighbors in the grid, interpolating the tidal values at the grid points for the appropriate time. Then we use bilinear spatial interpolation (e.g. *Press et al*., 1992) to compute the appropriate amplitude and phase of each tidal component at (x, y). Finally, we combine components using Equation 2.

At each gridded point, the amplitudes and phase of the tidal constituents can be calculated beforehand. Our algorithm is based on the pre- calculation of tides on a 1° by 1° grid globally (this can be performed on a HP-735 workstation of the GLAS Science Computing Facility, using the software described above with no attempt at streamlining the procedure or optimizing the software). When the pre-calculated results are stored on disk, a million points along a ground track, or about 5 orbits, can be calculated in 7 minutes through bilinear interpolation.

Figure 1 shows a grid block for the interpolation. The tidal loading L at point (x, y) is calculated by,

$$L(x, y) = (1-c_1)(1-c_2)L(x_1, y_1)+c_1(1-c_2)L(x_2, y_1)+c_1c_2L(x_2, y_2)+(1-c_1)c_2L(x_1, y_2)$$

$$c_1 = (x-x_1)/(x_2-x_1)$$

$$c_2 = (y-y_1)/(y_2-y_1)$$

Since the load tide varies smoothly, it can be interpolated in space and time with negligible error. This justifies our approach of tabulating load tide amplitudes and phases on a 1°×1° geographical grid. Then, to estimate tidal-loading displacements at any given time and any given point within Antarctica we use bilinear interpolation (e.g. *Press et al.*, 1992) to compute the appropriate amplitude and phase at that location, and use Equation 2.As a check, we compare calculated and interpolated values for a 180-day time series sampled at hourly intervals, starting January 1, 2001, at three locations: (66.6617°S, 140.0014°E), (70.5°S, 135.5°E), and (70.5°S, 45.5°E). The first point is near the coast, the other two are inland. The standard deviations of the residuals between calculated and interpolated values are 0.35 mm, 0.05 mm, and 0.03 mm, respectively. These are well within the accuracy requirements for correcting the measurements to be made by GLAS. In view of these results, it is clear that calculation of the tides at grid nodes

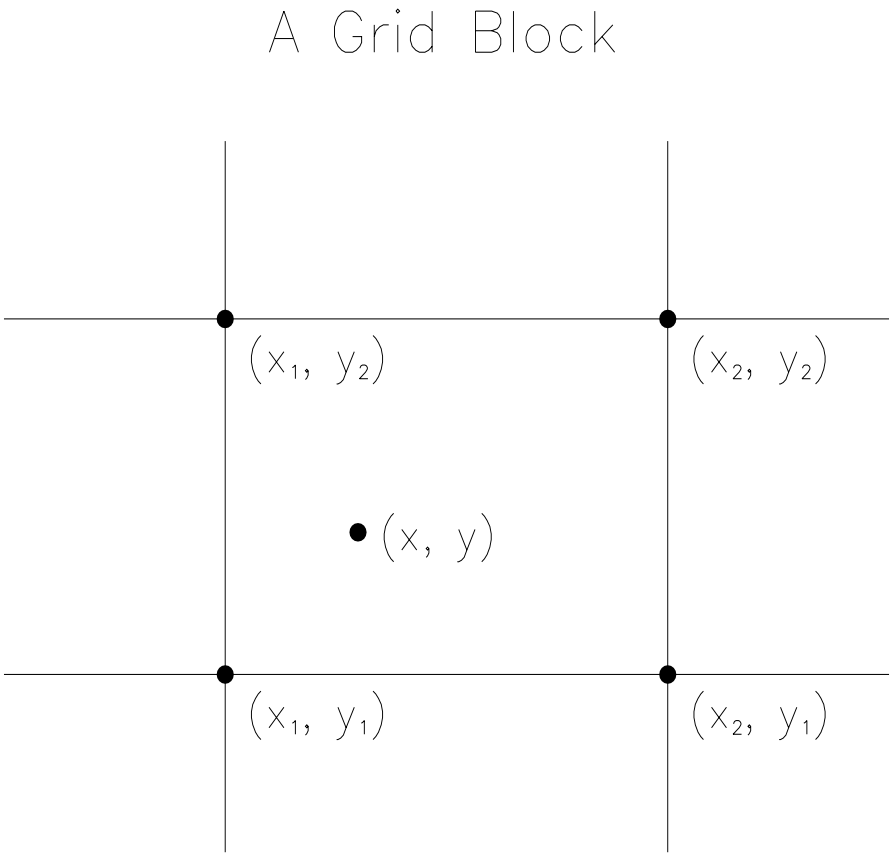

Figure 1: Geometry and notation for bilinear interpolation of ocean load tides.

need only be performed once during the time taken by the spacecraft to traverse the grid cell. This indicates that an effective strategy is to compute the corrections only at a relatively sparse set of points —say, every 15 seconds, that is every 600 shots, or every degree along track— and to interpolate using the shot count as the independent variable along track. This approach will work for any tidal correction, the only caveat being that the transitions from ocean to land environments and *vice versa* must be accounted for by keeping track of the intersections of the ground track with a sufficiently accurate map of the coastlines.

5.3 Discussion

In Equation 2 we accounted for the eight major tidal constituents (four semidiurnal waves: M_2, N_2, S_2, K_2; and four diurnal waves: K_1, O_1, P_1, Q_1) that have the largest contribution to tidal loading. We used the FES95.2 tide model to calculate the amplitude and phase of M_2, N_2, S_2, K_2, K_1, O_1, Q_1. TPXO.2 was used to calculate the amplitude and phase of P_1. We selected FES95.2 mainly because it is a readily available global ocean-tide model which includes the regions under the Ross, Filchner and Ronne Ice Shelves around Antarctica, regions which are of major concern

to the GLAS project.

As a validation of this approach, we compare the vertical displacement computed here to that obtained using amplitude and phase calculated by *McCarthy* (1992) following *Scherneck* (1991). At a test point (66.6617°S, 140.0014°E) in Antarctica, for a 180-day period starting from January 1, 2001, the difference between the two calculations is less than ±1.6 mm. McCarthy's results are estimated to be accurate at the ±3 mm level (*McCarthy*, 1992). Since we used a more recent, presumably improved tide model, we can assume that the accuracy of our calculation is at least as good.

The results show that the vertical tidal loading displacements are typically several centimeters over Antarctica. As expected, the amplitudes are higher along the coast and lower inland. The distribution of the *maximum* possible load tide over Antarctica (the sum of vertical displacements amplitude of eight tide constituents, which is what might be expected if all constituents ever happened to be in phase) is shown in Figure 2. It reaches a maximum value over Antarctica which exceeds 40 mm.

In practice, one sees the largest amplitudes when most of the constituents are in phase. For example at (66°S,100°E) the maximum amplitude is about 40 mm, but the total range of the displacement time series reaches only about 60 mm in the first ten years of the 21st century, not 80

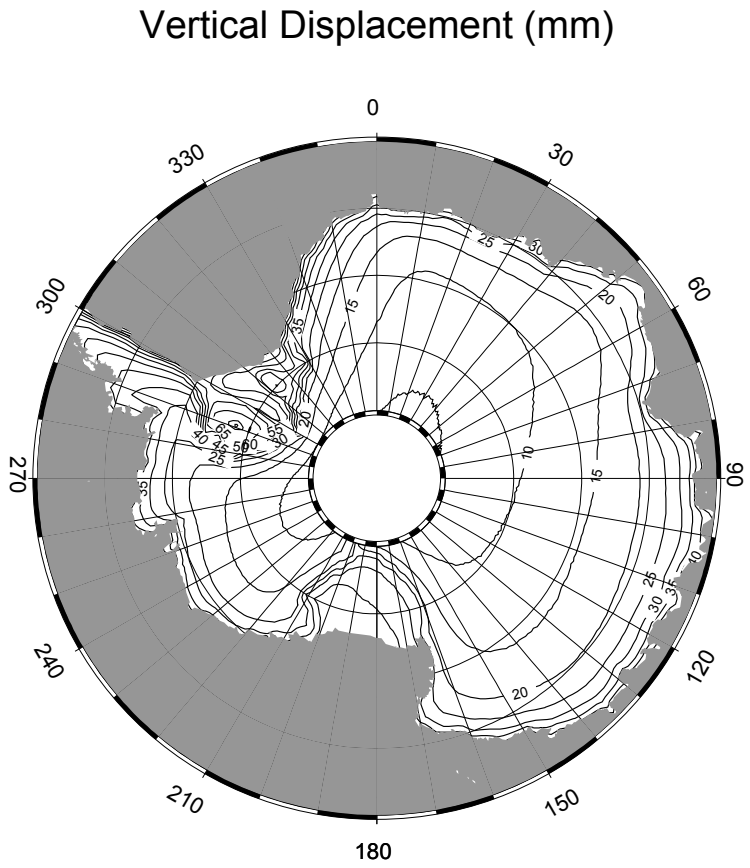

Figure 2: Contour map of maximum vertical displacement due to ocean tidal loading over Antarctica.

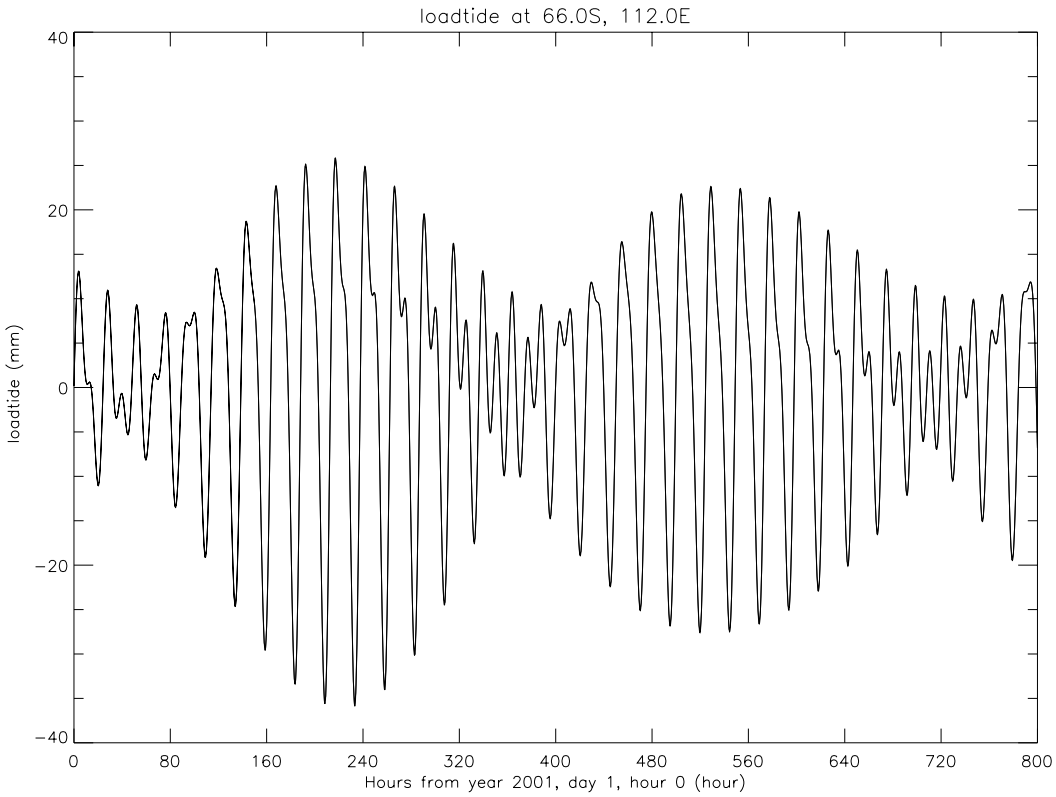

Figure 3: Comparison of load tide time series calculated at 1 hour intervals and at 12 minute intervals. This shows that temporal interpolation is justified.

mm. Figure 3 and Figure 4 are two examples showing the spatial and temporal variations of tidal loading. In Figure 3, two load tide time series are plotted. One is calculated at 1 hour intervals and the other at 0.2 hour intervals. They are indistinguishable, which demonstrates that temporal interpolation is fully justified.

Similarly, in Figure 4, there are two lines plotted: tidal loads calculated every degree and every half degree of longitude, respectively, at latitude 70°S. Again, the two cannot be distinguished. For a time series of 180 days starting from January 1, 2001, at one hour intervals, the standard deviation of the differences between the directly calculated value and the bilinear interpolated value are 0.35 mm, 0.05 mm and 0.03 mm for points at (66.6617°S, 140.0014°E), (70.5°S, 135.5°E), and (70.5°S, 45.5°E). This is good enough for GLAS tidal loading correction.

5.4 Tests of the Significance of the Loading Correction

A standard technique used in altimetry research is crossover analysis. This is done by comparing elevation estimates at successive passes (e.g. ascending and descending measurements) at a single location at the surface. We used a set of crossover points at high southern latitudes, provided by Dr. Schutz's group at University of Texas for an eight day repeat orbit scenario.

Figure 5 shows the tide loading effect over a crossover point at (67.7799°S, 123.1133°E)

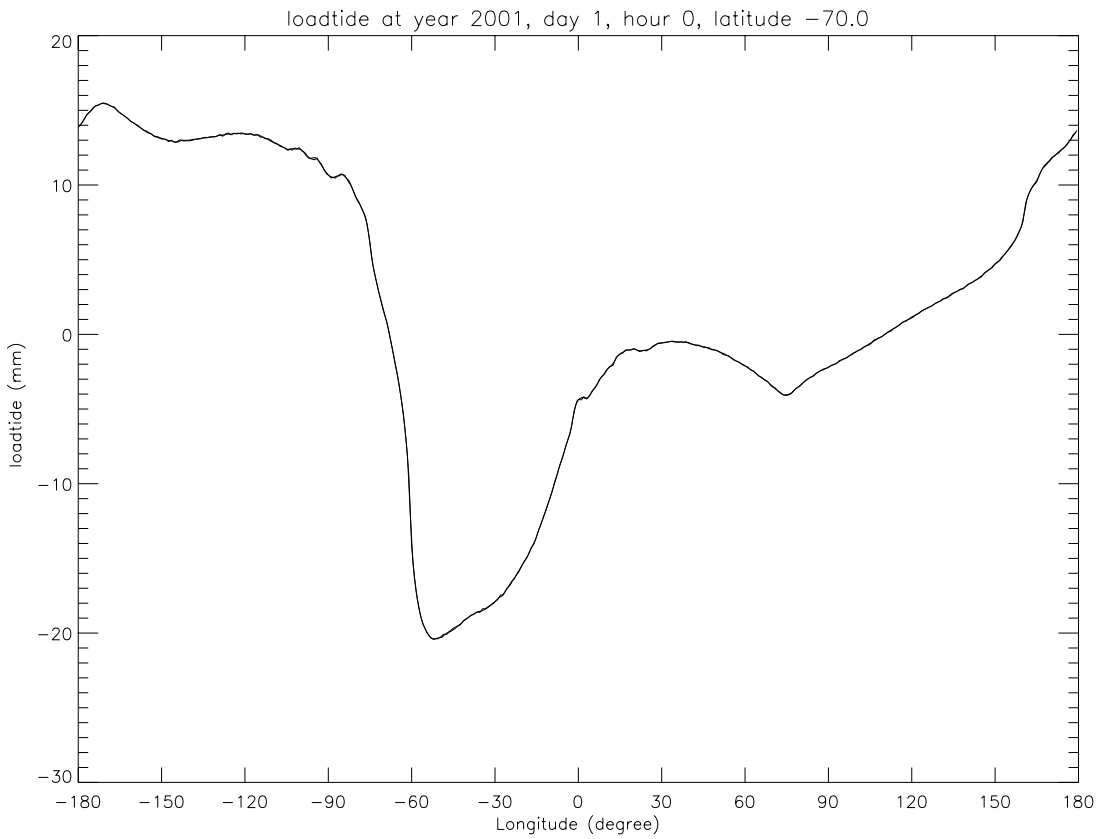

Figure 4. Vertical displacements at epoch 2001 00:00:00, along a small circle of latitude 70°S. Two estimates are shown, calculated at points separated by 1° and 0.5° longitude intervals, respectively. The excellent agreement justifies the practice of computing load tides on a coarse grid and interpolating bilinearly in space.

for the year 2001. Here we only consider the effect of tidal loading, in order to ascertain whether a beat pattern between tide frequencies and orbital periods might lead to aliased signals masquerading as systematic changes in elevation. Figure 5(a) shows the tidal load variation for the year 2001, starting on January 1, and calculated at one hour intervals. The apparent surface elevation changes for ascending and descending paths at the fiducial point are shown in Figures 5(c) and 5(e). Although individual differences could reach 30 mm, the differences for both ascending and descending passes have means of about zero and standard deviations of about 8 mm (Figures 5d and 5f). This means that if a sufficient number of measurements are used in calculating the surface elevation at this location, for this mission scenario, the bias would be small (several mm). The rms error for a single measurement is found to be less than ±10 mm. The error would be much smaller inland than along the coast.

It is difficult to assess the possibility of biases based on this single calculation. Indeed, there could be instances where the bias could be much more severe. By applying the tidal loading correction discussed above, such possible biases introduced by ocean tidal loading can be avoided. As shown above, ocean tide loading corrections are easily provided along the satellite

ground tracks. Applying these corrections will improve the accuracy of satellite altimeter measured surface elevations over polar regions, especially in the near coast area where the amplitude of the loadtide is larger than inland.

The histogram of these displacement values, shown in frame 5(b) shows that the distribution is significantly skewed at that location, although the mean over the 365-day cycle is very close to zero. This skewness is caused primarily by the near commensurability of the frequencies of certain tide components. (For instance, the histogram of values of the function $\cos\varpi t + \cos 2\varpi t$ is skewed, extending from a minimum of -1.2 to a maximum value of +2.) Furthermore, because this commensurability is nearly perfect for components k1 and k2, this phenomenon may persist with a beat period of many years. It should be noted that the degree of skewness is a function of time, and since it depends on the relative phases of the components, it depends also on location. If the beat period is in turn comparable to the repeat period of the sampling by GLAS, then it is possible for tidal loading signals to appear as small, but geographically coherent long term apparent changes in the average distribution of ice across the ice sheet. It is therefore important to perform this correction accurately. Table 2 shows the frequencies and amplitudes of the tides summed here at our test point, and Table 3 shows the beat periods of the most likely combinations of tides. The actual skewness and its actual geographical distribution is of course a result of the complex pattern of relative phases of all these components.

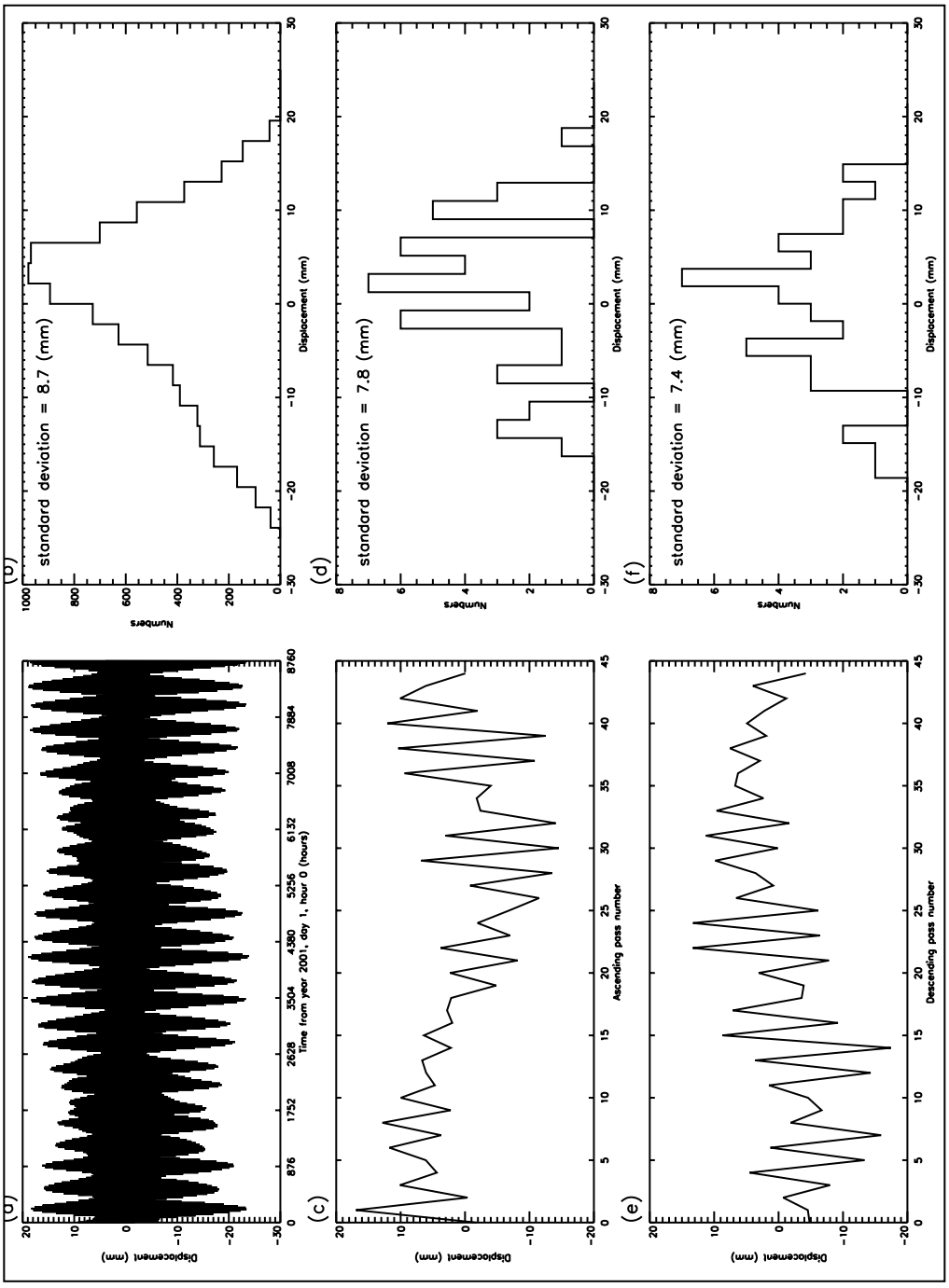

Figure 5: Tidal-loading variations in height and crossover analysis at 67°S, 102°E: (a) tidal-loading height variations for the year 2001; (b) surface-elevation changes at times of ascending-track passage; (c) surface-elevation changes at times of descending-track passage; (d), (e), and (f) histograms for the variations

Table 1: Approximate magnitudes of the components of the tide correction, and their uncertainties

Component	Magnitude	Uncertainty
Ocean tide (open ocean)	±50 cm	±10 cm
Ocean tide (coasts)	±2 m	±10 cm
Ocean tide (ice shelves)	±1 m*	± 40cm*
Long period ocean tide	±1 m (with long period)	few cm
Pole tide	< 2cm	few mm
Ocean-loading tide	±10 cm	< 0.5 cm
Solid Earth tide	±30 cm	±0.5 cm

Values from *Cudlip et al.* (1994).*For Amery Ice Shelf (*Phillips et al* (1999).

.

Table 2: Tide frequencies and vertical displacement at location (67.7799°S, 101.9368°E)

Tide	Frequency (Degree/hour)	Vertical Displacement (mm)
m2	28.9841	4.7
n2	28.4397	1.4
s2	30.0000	2.0
k2	30.0821	0.8
k1	15.0411	7.9
o1	13.9430	7.2
p1	14.9589	2.4
q1	13.3987	1.4

Table 3: Beat frequencies of selected pairs of tidal components

Tide Pairs	Repeat Period (years)
K1 ~ K2	infinity
K2 ~ S2	0.50
P1 ~ S2	0.50
P1 ~ K2	0.25

Appendix A – ICESat Mission Outline

The Ice, Cloud and land Elevation Satellite (ICESat) was launched on 13 January 2003. The Geoscience Laser Altimeter System (GLAS) instrument onboard ICESat made its first laser elevation measurement of the Earth on 21 February 2003 and its last on 11 October 2009. The three lasers employed by GLAS did not perform as long as expected, and following the failure of Laser 1 on 5 March 2003 the ICESat mission was modified to meet the requirement for capturing a multi-year time series of ice sheet elevations (Schutz et al., 2005). For the modified mission scenario, the spacecraft entered a 91-day repeat science orbit (compared to a planned 183-day repeat) and the lasers were activated for about 33 days of this 91-day repeat, two or three times per year. This campaign mode operation is summarized in Table A.1, and other significant parameters and events are listed in Table A.2. ICESat laser campaigns are designated by a laser number (L1, L2 or L3), followed by a letter in the sequence of operation. Following campaign L2f, attempts to restart any of the lasers were not successful. The spacecraft was put through a series of engineering tests in early 2010. De-orbit maneuvers were carried out in June and July 2010. The spacecraft was "passivated" on 14 August and reentered the Earth's atmosphere on 30 August 2010 over the Barents Sea northeast of Norway.

Table A.1: ICESat Laser Operation Campaigns

Campaign	Year	Day of year	Calendar Dates	Number of days (d)	Repeat orbit (d)	Repeat tracks[1]
L1a	2003	051-088	20 Feb-21 Mar	37	8	001-072 to 006-023
L2a	2003	268-277/ 277-322	25 Sep-4 Oct/ 4 Oct-21 Nov	54	8/ 91	028-088 to 029-100/ 1098 to 0421
L2b	2004	048-081	17 Feb-21 Mar	33	91	1284 to 0421
L2c	2004	139-173	18 May-21 Jun	34	91	1283 to 0434
L3a	2004	277-313	3 Oct-8 Nov	37	91	1273 to 0452
L3b	2005	048-083	17 Feb-24 Mar	35	91	1258 to 0426
L3c	2005	140-174	20 May-23 Jun	34	91	1275 to 0421
L3d	2005	294-328	21 Oct-24 Nov	34	91	1282 to 0421
L3e	2006	053-087	22 Feb-28 Mar	34	91	1283 to 0424
L3f	2006	144-177	24 May-26 Jun	33	91	1283 to 0421
L3g	2006	298-331	25 Oct-27 Nov	33	91	1283 to 0423
L3h	2007	071-104	12 Mar-14 Apr	33	91	1279 to 0426
L3i	2007	275-309	2 Oct-5 Nov	34	91	1280 to 0421
L3j	2008	048-081	17 Feb-21 Mar	33	91	1282 to 0422
L3k	2008	278-293	4 Oct-19 Oct	15	91	1283 to 0145
L2d	2008	330-352	25 Nov-17 Dec	22	91	0096 to 0423
L2e	2009	068-101	9 Mar-11 Apr	33	91	1286 to 0424
L2f	2009	273-284	30 Sep-11 Oct	11	91	1280 to 0084

[1] There are 119 tracks in the 8-day orbit and 1354 tracks in the 91-day orbit. Cycle numbers are included for the 8-day repeat periods.

Table A.2: Significant ICESat Parameters and Events by Campaign

Cam-paign	Year	Day of year	S/C orient-ation[1]	Start Beta' Angle (º)	End Beta' Angle (º)	Start Laser Infrared Energy (mJ)	End Laser Infrared Energy (mJ)	Mean footprint major axis (m)	Day of year – comments
-	2003	013	-	-	-	-	-	-	013 – launch
L1a	2003	051-088	-Y/+X	-45	-32	72	51	149	080 – yaw flip 085 – safe hold, adjust temperature
L2a	2003	268-277/ 277-322	+Y	51	69	80	55	100	277 – orbit change 286 – laser temperature anomaly 287, 302 – adjust temperature 311 – GPS solar flare anomaly
L2b	2004	048-081	+Y	54	40	57	33	90	
L2c	2004	139-173	-X	13	-4	33	5	88	142-147 – adjust temperature
L3a	2004	277-313	-Y	-48	-58	67	62	56	293 – adjust temperature
L3b	2005	048-083	-Y	-56	-45	68	54	80	054 – suspected amplifier bar drop, begin footprint anomaly[2] 068 – suspected amplifier bar drop
L3c	2005	140-174	+X	-20	-4	49	44	55	
L3d	2005	294-328	+Y	51	63	43	39	52	
L3e	2006	053-087	+Y	62	48	38	30	52	
L3f	2006	144-177	-X	20	4	30	30	51	149 - Energy jump up 2mJ
L3g	2006	298-331	-Y	-44	-54	30	24	53	310 – begin ITRF 2005
L3h	2007	071-104	-Y	-60	-47	24	21	56	
L3i	2007	275-309	+Y	32	46	22	20	57	
L3j	2008	048-081	+Y	74	62	20	16	59	
L3k	2008	278-293	+X	-28	-32	18	12	52	289 – Energy drop 4 mJ
L2d	2008	330-352	-Y	-45	-53	8	4	-	343-344 – adjust temperature, energy up 5 mJ
L2e	2009	068-101	-Y	-71	-59	6	2	-	094-095 – adjust temperature
L2f	2009	273-284	-X	20	25	4	2	-	
-	2010	242	-	-	-	-	-	-	242 – reentry

[1] The spacecraft is said to be in "Sailboat" mode for ±Y orientations and in "Airplane" mode for ±X orientations, where the direction indicates the solar panel orientation with respect to the spacecraft velocity using the GLAS coordinate frame.

[2] The footprint diameter during L3b changed from a mean of 54 m (day of year 048-053) to 84 m (055-068). The reason for the larger footprint size during the latter part of the campaign is unknown, although a suspected amplifier bar dropout occurs near the event.

Appendix B – Tide Models

All tide corrections mentioned below are applied to the elevation estimate provided in the GLA06 and GLA12-15 records. This means that if users are seeking elevation data that are not corrected for tides, then they must first un-apply the tide correction, a process referred to as "retiding" (Fricker and Padman, 2006). Retiding the data is particularly useful for looking for tide-induced signals over floating ice, such as in the ice shelf grounding zones. It is also imperative to do this for precise elevation change studies over ice shelves, so that a tide model that is more accurate in Antarctica could be applied (e.g. Pritchard et al., 2012).

The GOT99.2 model (Ray, 1999) was the initial ocean tide model applied to and provided with the ICESat/GLAS elevation data (GLA06, GLA12-15 products). Initial ocean tide reporting was at 2Hz (first and last valid shot in the 40 Hz packet). Ocean load tides were computed using SPOTL software (Agnew, 1996) from the GOT99.2 model and reported at 4Hz.

Solid-earth body tide was calculated based on NOAA's TIDPOT program to compute the tidal potential according to the expansion of Cartwright-Tayler-Edden, as given by Cartwright and Tayler (1971) and corrected in Cartwright and Tayler (1973). There were some changes made to this subroutine[11].

As the mission progressed, it became evident that the GOT99.2 tide model was not accurate enough, especially in Antarctica (King and Padman, 2005), and also that it was desirable to report ocean tides on a per-shot basis. There were also other realizations made about tidal and related corrections that were included in the later ICESat/GLAS data products for precise elevation change studies. As a result several changes in the tide processing occurred.

Summary of tide corrections at the start and end of ICESat mission

At the start of the ICESat mission, the following tide corrections were made to the elevation data and included in the records:

Standard tide corrections

Solid Earth tide *i_erElv*(2) @2Hz

Ocean tide corrections

Ocean tide (using GOT99.2) *i_ocElv*(2) @2Hz

[1] 1. Amplitudes (CS arrays) were updated to 1990 era per Woodworth. 2. Amplitudes for K1 and its sidebands (CS elements 213-215) were scaled by the ratio between the K1 Love number (0.52) and the overall second degree Love number (0.609), i.e. by 0.854. When the potential is later multiplied by the overall Love number, the result comes out correct (i.e. with correct K1 Love number). 3. CS elements 20 and 21 have been swapped, as suggested by Woodworth.

Ocean loading tide (based on GOT99.2 using SPOTL) *i_ldElv*(4) @4Hz

By the final release (Release 633), the following tide corrections were provided to the elevation data and included in the records:

Standard tide corrections

Solid Earth tide *i_erElv*(2) @2Hz

Equilibrium long-period tide *i_eqElv*(2) @2Hz

Pole tide *i_poleTide* @ 1Hz

Ocean tide corrections

Ocean tide (using TPX07.1) *i_ocElv*(40) @40Hz

Ocean loading tide (based on TPX07.0 using SPOTL) *i_ldElv*(4) @4Hz

Other information

Atmospheric pressure *i_Surface_pres*

Global mean atmospheric pressure *i_gASP @1Hz (GLA15 only)*

Chronological summary of changes made to ICESat tide corrections

September 2005 - GSAS V5.0 (Release 24)

GSAS 5.0 was a major release with extensive format changes to all products.

Addition

- Surface pressure (i_Surface_pres) added to GLA06,12-15 @1 Hz. This was reported in millibars of Mercury and derived from NCEP Final Analysis files. This is for estimation of the inverse barometer effect over the oceans and ice shelves.

June 25 2008 - GSAS V5.4 (Release 29)

GSAS 5.4 was a significant release with extensive changes including the incorporation of new tide models.

Addition

- Long period equilibrium tides were calculated made available on GLA06, and GLA12-15 at 2Hz (first and last valid shot). The value was included in the 40Hz ocean tide correction and applied to the elevations; it was provided on the GLA06 and GLA12-15 records at 2Hz so it could be un-applied by the user if desired.

Changes/Improvements

- Ocean tides were reported at 40Hz on the GLA06, GLA12-15 products.

April 2009 – GSAS V5.5 (Release 30)

Addition

- Added the global mean atmospheric pressure (globAvSrfPres) and the associated time (gASP_t) to the product headers on GLA06 and GLA12-15. Global mean pressure was computed as an average of the (over ocean) surface pressures globally every 6 hours from the NCEP forecasts.

August 2009 - GSAS V5.6 (Release 31)

Addition

- Added Pole Tide i_polTide(2) to GLA06, GLA12-15 over oceans at 2Hz. This is only computed/applied if the landmask is set to ocean.

March 2011 - GSAS V6.0 (Release 33)

Changes/Improvements

- Ocean tide model was changed from GOT99.2 to TPXO7.1 (Egbert and Erofeeva, 2002) on the GLA06, GLA12-15 products.
- Ocean load tide calculated based on TPX07.0 using SPOTL
- Corrected the description of i_poleTide
- Global mean surface pressure (i_gASP) added to GLA15 product @1Hz

References

Agnew, D. C., SPOTL: Some programs for ocean-tide loading, SIO Ref. Ser. 96-8, 35 pp., Scripps Inst. of Oceanogr., La Jolla, Calif., 1996

Baker, T. F., Method of tidal loading computation, MAREES TERRESTRES. BULLETIN D'INFORMATIONS, 94, 6365-6373, 1985.

Bentley, C. R. and D. D. Sheehan. Comparison of altimetry profiles over East Antarctic from Seasat and Geosat, an interim report. Z. Gletscherkd, Glazialgeol., 26(1), 1-9, 1992.

Brenner, A. C., R. A. Bindschadler, R. H. Thomas, and H. J. Zwally, Slope-induced errors in radar altimetry over continental ice sheets. J. of Geophys. Res., 88(c3), 1,617-1,623, 1983

Cartwright, D. E. and Tayler, R. J. (1971), New Computations of the Tide-generating Potential. *Geophysical Journal of the Royal Astronomical Society*, 23: 45–73. doi: 10.1111/j.1365-246X.1971.tb01803.x

Cartwright, D. E. and Edden, A. C. (1973), Corrected Tables of Tidal Harmonics. *Geophysical Journal of the Royal Astronomical Society*, 33: 253–264. doi: 10.1111/j.1365-246X.1973.tb03420.x

Cudlip, W., D.R. Mantripp, C.L. Wrench, H.D. Griffiths, D.V. Sheehan, M. Lester, R.P. Leigh and T.R. Robinson. Correction for altimeter low-level processing at the Earth Observation data Centre (EODC). International Journal of Remote Sensing, 15, No. 4, pp 889-914.

Doodson, A. T., The analysis of tidal observations. Phil. Trans. Roy. Soc. Lond., 227, 223-279, 1928

Eanes, R. J., Diurnal and semidiurnal tides from TOPEX/POSEIDON altimetry, Eos Trans. AGU, 1994 Spring Meeting Suppl., 108, 1994.

Egbert, G. D., A. F. Bennett, and M. G. G. Foreman, TOPEX/POSEIDON tides estimated using a global inverse model, J. Geophys. Res., 99, 24821-24852, 1994.

Egbert, G.D., and S.Y. Erofeeva, 2002. Efficient inverse modeling of barotropic ocean tides, *J. Atmos. Oceanic Technol.*, **19**(2), 183-204., http://www.esr.org/polar_tide_models/Model_TPXO71.html, last accessed June 2012.

Farrell, W. E., Deformation of the Earth by surface loads, Rev. Geophysics and Space Phys., 10, 761-797, 1972.

Fricker, H. A., L. Padman (2006) Ice shelf grounding zone structure from ICESat laser altimetry, *Geophys. Res. Letts.*, 33, L15502, doi:10.1029/2006GL026907.

Haines, B. J., G. H. Born, R. C. Williamson, and C. J. Koblinsky. Application of the GEM-T2 gravity field to altimetric satellite orbit computation. J. Geophys. Res. 99(c8), 16,237-16,254, 1994.

Jacobs, S. S., Is the Antarctic ice sheet growing? Nature, 36029-33, 1992.

King, M. A., and L. Padman (2005), Accuracy assessment of ocean tide models around Antarctica, *Geophys. Res. Letts.*, 32, L23608, doi:10.1029/2005GL023901.

Le Provost, C., M. L. Genco, F. Lyard, P. Vincent, and P. Canceil, Spectroscopy of the world ocean tides from a finite element hydrodynamic model, J. Geophys. Res., 99, 24777-24797, 1994.

Le Provost, C., A. F. Bennett, and D. E. Cartwirght, Ocean tides for and fromTOPEX/POSEIDON, Science, 267, 639-642, 1995.

Le Provost, C., F. Lyard, J. M. Molines, M.L. Genco and F. Rabilloud. A hydrodynamic ocean tide model improved by assimilating a satellite-altimeter-derived data set, J. Geophys. Res., 103, 5513-5529, 1998.

Lingle, C. S., L. Lee, H. J. Zwally, and T. C. Seiss. Recent elevation increase on Lambert Glacier, Antarctic, from orbit crossover analysis of satellite radar altimetry. Ann. Glacial., 20, 26-32, 1994.

McCarthy, D. D. (ed), IERS Technical Note 13, 1992.

Oerlemans, J. Possible changes in the mass balance of the Greenland and Antarctic ice sheets and their observations, projections and implications. Edited by R. A. Warrick, E. M. Bar-row and T.M. L. Wigley. Cambridge University Press. 424 pp. 1993.

Partington, K. C., W. Cudlip, and C. G. Rapley. An assessment of the capability of the sat-ellite radar altimeter for measuring ice sheet topographic change. Int. J. Remote Sensing, 12(3), 585-609. 1991.

Phillips, H.A, I. Allison, R. Coleman, G. Hyland, P.J. Morgan and N.W. Young. Compari-son of ERS satellite radar altimeter heights with GPS-derived heights on the Amery Ice Shelf, East Antarctica. Annals of Glaciology, 27, 19-24, 1998.

Phillips, H.A, G. Hyland, R. Coleman and N.W. Young. Digital Elevation Models for the Lambert Glacier-Amery Ice Shelf system, East Antarctica, from ERS-1 satellite radar altimetry. Submitted to Journal of Glaciology, August 1999.

Press, W. H., S. A. Teukolsky, W. T. Vetterling, and B. P. Flannery, Numerical Recipes in C. Cambridge University Press, New York, 994 pp., 1992.

Pritchard, H.D., S.R.M. Ligtenberg, H.A. Fricker, D.G. Vaughan, M.R. van den Broeke and L. Padman (2012) Antarctic ice sheet loss driven by basal melting of ice shelves, *Nature*, 484, 502-505.

Ray, R. 1999. A global ocean tide model from TOPEX/POSEIDON Altimetry: GOT99.2, NASA/TM-1999-209478, Goddard Space Flight Center, Greenbelt, MD, http://ntrs.nasa.gov/archive/nasa/casi.ntrs.nasa.gov/19990089548_1999 150788.pdf, last accessed June 2012.

Ridley, J. K. and K. C. Partington. A model of satellite radar altimeter return from ice sheets. Int. J. Remote Sensing. 9(4), 601-624, 1988.

Rignot, E. Radar interferometry detection of hinge-line migration on Rutford Ice Stream and Carlson Inlet, Antarctica. Annals of Glaciology, 27, 25-32, 1998.

Rignot, E., L. Padman, D.R. MacAyeal and M. Schmeltz. Analysis of sub-ice-shelf tides in the Weddell Sea using SAR imterferometry. Submitted to J. Geophys. Res., 1999.

Robertson, R., L. Padman and G. Egbert. Tides in the Weddell Sea. In Ocean, Ice, and Atmosphere: Interactions at the Antarctic Continental Margin, Antarctic Research Series, 75, pp. 341-369, 1998.

Scherneck, H. G., A parameterized solid earth tide model and ocean tide loading effects for global geodetic baseline measurements, Geophys. J. Int., 106, 677-694, 1991.

Schutz, B. E. Geoscience Laser Altimeter System. MTPE/EOS Reference Handbook. 123-134, 1995.

Schutz, B.E.; Zwally, H.J.; Shuman, C.A.; Hancock, D.; DiMarzio, J.P. Overview of the ICESat Mission. *Geophysical Research Letters* 2005, 32, L21S01 (DOI:10.1029/2005GL024009).

Schwiderski, E. W., On charting global ocean tides, Rev. of Geophys. and Space Phys.,18. No. 1, 243-268, 1988.

Shum, C.K., P.L. Woodworth, O.B. Anderson, G.D. Egbert, O. Francis, C. King, S.M. Klosko, C. Le Provost, X. Li, J-M Molines, M.E. Parke, R.D. Ray, M.G. Schlax, D. Stammer, C.C. Tierney, P. Vincent and C.I. Wunsch, Accuracy assessment of recent ocean tide models, J. Geophys. Res., 102, 25173-25194, 1997.

Vaughan, D.G., Investigating tidal flexure on an ice shelf using kinematic GPS. Annals of Glaciology, 20, 372-376, 1994.

Vaughan, D.G., Tidal flexure at ice shelf margins. J. Geophys. Res., 100(B4), 6213-6224, 1995

Warrick, R. A., Climate and sea level change: a synthesis. Climate and sea level change: Observations, projections, and implications. Edited by R. A. Warrick, E. M. Barrow and T. M. L. Wigley. Cambridge University Press. 424 pp. 1993.

Warrick R. A. and J. Oerlemans. Sea level rise. Climate change, the ICPP Scientific Assessment. Edited by J. T. Houghton, G. T. Jenkins and J. J. Ephraums. Cambridge University Press. 365, pp. 1990.

Wessel, P., and W. H.F. Smith. A global, self-consistent, hierarchical, high-resolution shoreline database, J. Geophys. Res., 101, 8741 - 8743, 1996.

Yi, D. and C. R. Bentley. A retracking algorithm for satellite radar altimetry over an ice sheet and its applications. Glaciers, Ice Sheets, and Volcanoes: A Tribute to Mark F. Meier. Edited by S. C. Colbeck. U.S. Army Cold Regions Research and Engineering Laboratory, Special report 96, 27, 112-120, 1997.

Yi, D., C. R. Bentley, and M. D. Stenoien. Seasonal variation in the height of the East Antarctic ice sheet. Ann. Glaciol., 24, 191-198, 1997.

Zwally, H. J., Growth of Greenland ice sheet: interpretation. Science, 246(4937), 1,589-1,591, 1989.

Zwally, H. J., A. C. Brenner, J. A. Major, R. A. Bindschadler, and J. G. Marsh. Growth of Greenland ice sheet: Measurement. Science, 246 (4937), 1,587-1,589, 1989.

Zwally, H. J., A. C. Brenner, J. A. Major, T. V. Martin and R. A. Bindschadler. Satellite radar altimetry over ice. Vol. 1, Processing and corrections of Seasat data over Greenland, Wash-ington, DC, National Aeronautics and Space Administration. (NASA Ref. Pub. 1233, 1.)